geosciences

MDPI

Article

Garnet Geochemistry and Lu-Hf Geochronology of a Gold-Bearing Sillimanite-Garnet-Biotite Gneiss at the Borden Lake Belt

Daniel LaFontaine [1], Audrey Bouvier [2,3,*] and Mary Louise Hill [1]

[1] Department of Geology, Lakehead University, Thunder Bay, ON P7B 5E1, Canada; dlafontaine@probemetals.com (D.L.); mlhill@lakeheadu.ca (M.L.H.)
[2] Bayerisches Geoinstitut, Universität Bayreuth, 95447 Bayreuth, Germany
[3] Department of Earth Sciences, University of Western Ontario, London, ON N6A 5B7, Canada
* Correspondence: audrey.bouvier@uni-bayreuth.de

Abstract: The Kapuskasing Structural Zone transects the Wawa and Abitibi greenstone belts in the Superior province of the Canadian Shield. At the southern margin of the Kapuskasing Structural Zone (KSZ), the Borden Gold deposit hosts low-grade-gold mineralization within upper amphibolite- to granulite-facies sillimanite-garnet-biotite gneisses. Here, we present the geochemistry and Lu-Hf geochronological studies of a gold-hosting garnet-bearing gneiss to constrain the formation history of the deposit and regional geological history. The garnet is almandine-rich, and contains inclusions of quartz, biotite, pyrite, and zircon. The absence of chemical zoning in garnet is likely due to intracrystalline diffusion at peak metamorphic temperatures. The ^{176}Lu-^{176}Hf internal isochron of two garnet fractions and three corresponding whole-rock splits from a gneissic unit yield a precise internal isochron age at 2629.0 ± 4.3 Ma (MSWD = 0.66), with an initial ^{176}Hf/^{177}Hf = 0.281210 ± 0.000010 corresponding to an εHfi = +4.1. This signature suggests a mafic source, which was derived from a long-term depleted reservoir, for this metasediment. The Lu-Hf age is consistent with the youngest age population of zircons from the paragneisses, which were previously dated in the area. Our results thus provide upper constraints on the timing of retrograde upper-amphibolite metamorphism and gold mineralization at Borden.

Keywords: Lu-Hf garnet geochronology; Kapuskasing Structural Zone; Borden Lake Belt; Gold deposit; granulite-facies metamorphism; sillimanite-garnet-biotite gneiss

Citation: LaFontaine, D.; Bouvier, A.; Hill, M.L. Garnet Geochemistry and Lu-Hf Geochronology of a Gold-Bearing Sillimanite-Garnet-Biotite Gneiss at the Borden Lake Belt. *Geosciences* **2022**, *12*, 218. https://doi.org/10.3390/geosciences12050218

Academic Editors: Ian Smith and Jesus Martinez-Frias

Received: 14 April 2022
Accepted: 18 May 2022
Published: 23 May 2022

1. Introduction

The Superior province is one of the oldest cratons in the world. It is hypothesized to have been assembled by the end of the Archean through the accretion of terranes now represented by subprovinces [1,2]. The Abitibi and Wawa subprovinces are interpreted to be the last terranes accreted between 2750–2670 Ma [1] during northward subduction during the Kenoran Orogeny [2]. The Borden Gold deposit (Ontario, Canada) is located at the southern margin of the Archean Kapuskasing Structural Zone (KSZ), a structurally controlled region of granulite- and upper amphibolite-facies metamorphic rocks. The fault-bound KSZ displays many structural characteristics that are prospective for gold endowment although, owing to the high grade of metamorphism, very little historical exploration has been undertaken in this unconventional setting. In 2010, Probe Mines Ltd. discovered a 91 m intercept of low-grade gold (2.0 g/t Au) in the Borden Lake Belt, an east-west-striking lithological assemblage consisting of paragneiss and orthogneiss. Fast-paced exploration developed this intercept into the multi-million-ounce Borden Gold deposit that is currently being mined by Newmont.

Following the discovery by Probe Mines Ltd. in 2010, the project advanced rapidly and consequently has sparked significant exploration activity in the surrounding region. At Borden, gold mineralization is associated with the metamorphic sillimanite-garnet-biotite gneiss unit. The geochemical and Lu-Hf geochronological analyses of the gold-hosting

garnet-bearing gneiss were investigated to constrain the formation history of the deposit and regional geological history. Its unusual setting has brought up many questions about the geologic history and the relationship to gold mineralization as it is situated directly west of the world-class Porcupine-Destor gold trend. Previous geochronological studies surrounding the KSZ and more specifically the Borden Lake Belt (BLB) have focused on understanding the timing of the mafic volcanism, (meta)conglomerate deposition, and intrusive bodies, but not subsequent metamorphism. The thermal conditions and timing of formation of gold mineralization at the Borden Gold deposit were previously constrained by U-Pb geochronology of zircons of the host rocks, (e.g., [2–4]). Zircon U-Pb in situ measurements have sometimes been interpreted along with Hf isotopic measurements to constrain their source reservoirs as well as their formation ages in the region [5]. In comparison, limited whole-rock Hf or Nd isotopic analyses of Archean metasediments from the Abitibi are available in the literature to place constraints on their protoliths and history of accreted terranes, (e.g., [6,7]).

The drill core and channel sampling from the "Discovery Outcrop" has provided a critical sample suite for microstructural analysis and scanning electron microscopy which have been described elsewhere [8]. To provide constraints on the timing of peak metamorphism and further constrain the gold mineralization at Borden, we here present the geochemical and Lu-Hf geochronological records from the gold-hosting sillimanite-garnet-biotite gneiss sample FD 01340 from the Discovery Outcrop at the Borden Gold deposit. We also report additional Lu-Hf whole-rock isotopic data and discuss the potential source of metasediments found at Borden Lake.

2. Geological Context

2.1. The Kapuskasing Structural Zone

The Kapuskasing Structural Zone (KSZ) (Figure 1) is a 500 km long belt that strikes NNE to SSW and crosscuts the east-west trend of the adjacent Abitibi and Wawa Subprovinces. It represents a deep crustal assemblage that has been exhumed along a major crustal structure. The grade of metamorphism ranges from upper amphibolite to granulite facies, and the presence of a large anorthosite complex, the Shawmere anorthosite, is consistent with exhumation from the deep crust. Northeast–southwest lineaments of the Thompson Belt, the Wollaston Lake Belt, and the Kapuskasing Structural Zone have been regarded as members of a genetically related set of shear zones formed during the late Archean in the interior of a large continental mass [9–11]. Within the KSZ, various garnet-biotite and garnet-pyroxene geothermometers and geobarometers yield apparent temperature ranges from <600 °C in the west to locally >800 °C [3]. Percival [3] previously used garnet-biotite geothermometry to calculate temperature ranges that are between 580 °C to 825 °C for areas in the KSZ and more specifically 630 °C ± 50 °C proximal to the Borden gold zone.

The KSZ is composed of gneisses in the upper amphibolite to granulite facies with the metamorphic grade decreasing abruptly to greenschist facies in the Abitibi Subprovince to the southeast, across the Ivanhoe Lake Deformation zone. A gradual transition from granulite- to amphibolite-facies metamorphism occurs through the Wawa Gneiss Domain across the Saganash Lake Fault to the northwest [12].

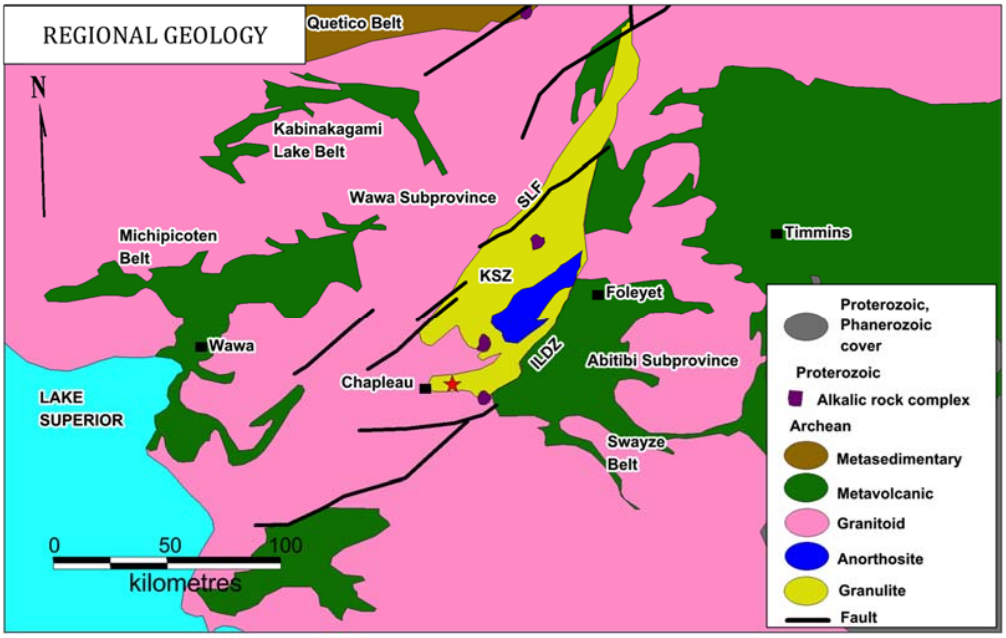

Figure 1. Regional map of the Kapuskasing Structural Zone, Wawa and Abitibi Subprovinces. The location of the Borden Gold deposit is denoted by the red star (modified after Heather et al. [13]; and from Probe Mines Ltd.).

2.2. The Borden Lake Belt

The Borden gold property is located within the Borden Lake Belt (BLB) near the southern margin of the KSZ (Figure 1). The BLB is a 5 km by 25 km east–west striking lithological assemblage, consisting of paragneiss (metapelites and metaconglomerate), orthogneiss (metavolcanic rock), felsic and mafic gneisses, all of which underwent high-grade metamorphism from upper amphibolite to granulite facies. Mapping by Moser [14] describes the western portion of the Borden Lake Belt as a tight synform that preserves sedimentary and volcanic structures. In contrast to the amphibolite-facies units in the western BLB, the eastern metavolcanic rocks are interlayered with felsic orthogneiss and have granulite-facies mineralogy. Moser [14] also notes areas with relict granulite-facies assemblages in retrogressed metavolcanic rocks to the west and north. Amphibolite and garnet-amphibolite gneiss extending from the BLB margin inward are described as metavolcanic rocks with preserved deformed pillow structures with garnetiferous selvedges [2].

The Borden gold zone is defined by lithological, structural, density, and seismic velocity changes reflecting the transition from granulite to amphibolite facies [14,15]. Moser [14] observed that the oblique transect of the dominant east–west lithological trend allows for lithological and structural correlation between deep-crustal (KSZ) and the mid-crustal levels of the Borden Lake Belt [12,14].

Percival and Krogh [3] dated a granodiorite that crosscuts the mafic gneiss at the southern margin of the KSZ at 2677 +5/−3 Ma, which is implied to establish a minimum age for mafic volcanism. Published zircon estimations derived from metaconglomerate matrix yield a maximum age for metaconglomerate deposition at the Borden Belt of 2671 ± 12 Ma [2] and 2667 ± 2 Ma [4]. The Borden Lake metaconglomerate does not host gold mineralization and is not directly associated with mineralized lithologies on the Borden property.

Detrital zircon dating by Moser et al. [2] utilizes younger U-Pb ages of zircon rims compared to the corresponding cores (~2.85–2.67 Ga) to constrain a lower age bracket of 2659 ± 8 Ma for the burial of Borden Lake metasediments in the lower crust. The zircon rims have concentric changes in U-Pb ages, oxygen isotope values, and trace elements [2]. Moser et al. [2] conclude that multi-stage radial growth of zircon occurred until 2.58 ± 0.01 Ga. Rather than short-lived in situ recrystallization, the authors suggest that growth would have occurred around detrital zircon cores for as much as 80 m.y. During this period,

the apparent Ti-in-zircon temperatures vary between 706 °C and 660 °C. Metamorphic growth events appear to have been most frequent at ca. 2620 Ma, when temperatures were above 650 °C. These events coincide with boudinage in the lower crust and crustal-scale fluid flow along with brittle structural breaks at higher levels [4]. Evidence for late Archean (ca. 2630 Ma) fault activity also exists along the Ivanhoe Lake fault zone [16]. Therefore, deformation, metamorphic temperatures, and garnet growth may have been near-synchronous and protracted until this period.

2.3. The Borden Gold Deposit

An assortment of lithologies, each exhibiting structural and textural variations, are host to gold in various concentrations at the Borden Gold deposit (Figure 2). There are a few occurrences of visible gold in the drill core but more gold has been identified by microstructural analysis [8]. Gold-hosting lithologies on the Borden property are sillimanite-garnet-biotite gneiss (logged as garnet biotite schist), amphibolite (±garnet) (logged as amphibolite), biotite-quartzo-feldspathic gneiss (logged as quartzofeldspathic gneiss or biotite schist) and deformed quartz veins. The sillimanite-garnet-biotite gneiss is associated with economic gold mineralization on the Borden Gold property and is the focus of this study (Figure 2). At the macroscopic scale, gold mineralization is associated with the margins of competent lithons. Microstructural patterns are analogous to macroscopic lithological relationships, with evidence of gold mineralization surrounding competent micro-lithons.

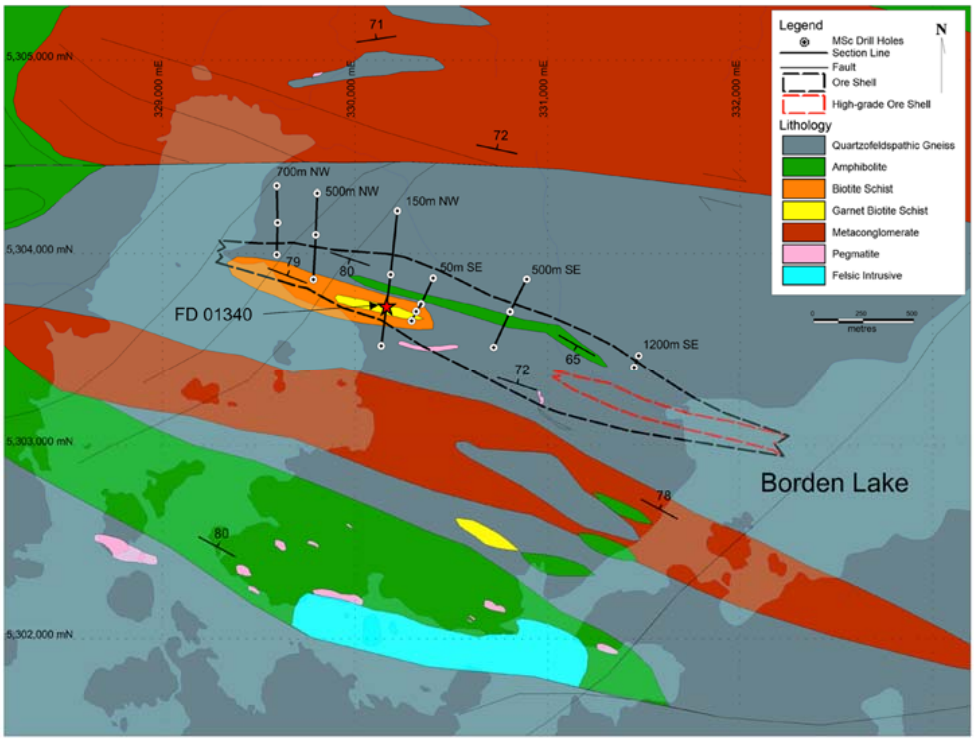

Figure 2. Map of the Borden Lake Belt geology overlain on a map of land and lakes, produced from Probe Mines Limited geologic mapping between 2012–2015. The ore zone is projected to surface in black and red stippled lines. Section lines highlight reassessed drill hole locations that were utilized for thesis research core reassessment and sampling. Core logging and 2D cross-section interpretations indicate the lateral continuity of the sillimanite-garnet-biotite gneiss, while also highlighting the variability in thickness of this unit throughout the property. Core logging has also identified multiple layers of the sillimanite-garnet-biotite gneiss separated by quartzo-feldspathic gneiss and amphibolite units.

The sillimanite-garnet-biotite gneiss is typically composed of quartz, plagioclase, potassium feldspar, biotite, garnet and sillimanite with accessory minerals magnetite,

zircon, gold, pyrite, and pyrrhotite. The unit is moderately to strongly foliated, defined by parallel alignment of biotite. The outcrop displays biotite-rich (20% to 35%) layers defining foliation that anastomose around competent quartzo-feldspathic or amphibolite lithons (Figure 3a). Garnet is red-colored, subhedral, millimeter-sized, and comprises up to 15% of the modal mineral abundance. Under plane-polarized light, the garnet is pink to colorless and may contain inclusions of quartz, biotite, and pyrite. Biotite often surrounds garnet forming a complete or partial corona with some occurrences of biotite forming asymmetric tails (Figure 3b). The strain shadows adjacent to the garnet commonly have increased quartz or sulfide content. Sillimanite is observed in the petrographic analysis as both fibrolite and coarse sillimanite (Figure 3c). The fibrolite occurs as small grains on quartz and mica. Fibrolite grows as small clusters of needles in a fan shape. Some prismatic coarse sillimanite grains can be observed as part of large lithons surrounded by biotite, K-feldspar, and quartz.

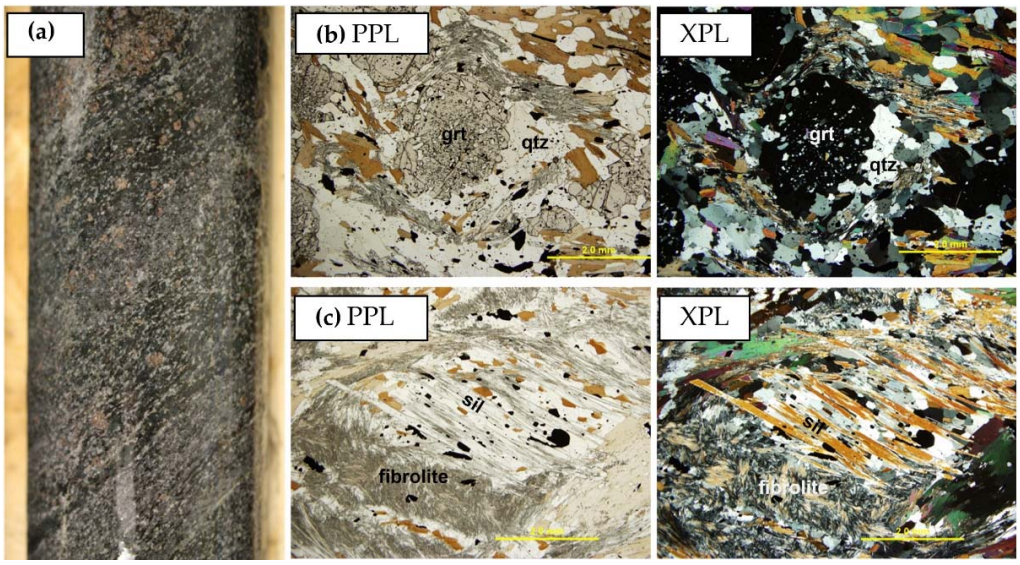

Figure 3. (**a**) Strongly foliated garnet-biotite schist with garnet porphyroclasts; logging core is 5 cm in width. (**b**) Sillimanite-garnet-biotite schist, garnet at center surrounded by biotite and sillimanite with quartz in the low-strain zone (right-center) from sample FD 01342 (176 ppb Au). (**c**) Sillimanite-garnet-biotite schist, with prismatic sillimanite at the centre and retrograde fibrolite in the bottom left from sample FD 01339 (1440 ppb Au). PPL = plane-polarized light; XPL = cross-polarized light.

Parallel alignment of platy minerals is a marker for mineralized lithologies at the Borden property. Stable retrograde amphibolite-facies minerals typically define foliation indicating synchronous retrograde metamorphism and deformation processes. The foliated sillimanite-garnet-biotite gneiss appears to be ductilely deformed around the competent biotite-quartzo-feldspathic gneiss. The subparallel alignment of biotite defines a moderate foliation, which could indicate a lower strain environment allowing the crystals to attain larger dimensions. A coarse-grained and chaotic biotite texture is common, and the foliation can anastomose around competent units. The thin necks of stretched sillimanite-garnet-biotite gneiss preferentially host quartzo-feldspathic gneiss units. This lithological relationship appears to be a favorable location for gold mineralization.

The diminution of garnet crystal shape, abundant internal fractures, and setting within a strongly foliated groundmass suggest that deformation occurred during and after garnet growth. The strong foliation of the surrounding groundmass is deflected around the garnet, suggesting that the competent garnet behaved as a porphyroclast during subsequent ductile deformation. Coarse biotite, quartz, or gold mineralization are also common in the low-strain zone adjacent to the garnet.

The dominant mineralogy of the amphibolite (±garnet) is quartz, plagioclase, biotite, hornblende, and garnet with accessory minerals of gold, pyrite, and pyrrhotite. This unit is

weakly to strongly foliated and ranges from fine- to medium-grained. Foliation is defined dominantly by hornblende, minor biotite, and sulfides. A unique feature of the amphibolite is the rare presence of microlithons containing clinopyroxene and orthopyroxene. These appear to be relict domains of granulite-facies mafic gneiss, indicating that the amphibolite-facies metamorphism is retrograde. Further evidence of retrograde metamorphism is illustrated by the replacement of granulite-facies minerals by hornblende in [8]. The minerals have abundant microfractures and irregular grain boundaries. Surrounding these relict pyroxene lithons are moderately to strongly aligned euhedral hornblende with garnet, plagioclase, and quartz.

2.4. Sequence of Polymetamorphism

What sets the mineralized units on the Borden property apart from the regional granulite-facies metamorphism of the Kapuskasing Structural Zone is the small quantity of granulite-facies assemblages preserved within dominantly retrograde amphibolite-facies assemblages. On the Borden gold property, mineralized units preserve vestiges of unstable granulite-facies minerals within stable amphibolite-facies assemblages. The retrograde amphibolite-facies metamorphism observed in the gold-hosting sillimanite-garnet-biotite gneiss appears to be significant to gold mineralization.

Relict lithons and minerals are preserved in some rocks in the area indicating peak granulite-facies metamorphism. In metapelitic rocks, the granulite facies is characterized by the absence of muscovite and the presence of sillimanite, cordierite, garnet, quartz, K-feldspar, and orthopyroxene. In the sillimanite-garnet-biotite gneiss, coarse sillimanite and poikiloblastic K-feldspar represent granulite-facies metamorphism at temperatures above the second sillimanite isograd or K-feldspar and sillimanite isograd. The absence of muscovite in the garnet-biotite schist indicates that muscovite, if present, was completely consumed during this prograde granulite-facies metamorphic reaction. The presence of garnet, orthopyroxene, and clinopyroxene in the garnet amphibolite indicates peak granulite-facies metamorphism.

The occurrence of sillimanite-garnet-biotite gneiss with quartz, feldspar, biotite, almandine garnet, fibrolite, and coarse sillimanite is consistent with upper amphibolite-facies metamorphism. In many samples of sillimanite-garnet-biotite gneiss, there is both fibrolite and coarse sillimanite (Figure 3c). Fibrolite is unlikely to be stable at granulite-facies temperatures and would be expected to recrystallize as coarse sillimanite. Therefore, the presence of fibrolite suggests secondary growth of sillimanite at amphibolite-facies temperatures during retrograde metamorphism.

3. Materials and Methods

3.1. Polished Thin Section Analysis

A polished thin section of sample FD 01340 was prepared at Lakehead University's Rock Preparation Laboratory. Petrographic and microstructural analysis (Figures 3 and 4a) was conducted at Lakehead University using an Olympus BX51 transmitted and reflected light microscope with an attached Nikon 8 MP microscopic camera for photomicrographs. Full petrographic analysis with modal mineral abundances based on visual inspection, mineral association, and mineralization can be found in LaFontaine [8].

Table 1. Spot EDS analyses on individual garnet core and rim locations of one garnet from sample FD 01340, including calculated oxide values, per formula unit values, and garnet end-member proportions. Ti was below detection limits.

	Grt Core 1	Grt Core 2	Grt Core 3	Grt Rim 1	Grt Rim 2	Grt Rim 3
Oxide (wt%)						
MgO	2.58	3.47	3.93	3.24	2.28	2.94
Al_2O_3	20.7	21.3	20.7	20.9	20.8	21.2
SiO_2	35.7	37.7	36.5	37.3	36.5	37.0
CaO	1.18	1.13	1.13	1.23	0.81	1.15
MnO	6.74	6.18	6.33	7.47	8.42	7.41
FeO	33.61	30.2	30.0	29.4	31.0	29.8
Total	100.5	100.0	98.6	99.5	99.9	99.6
Cations per formula unit						
Mg	0.31	0.41	0.48	0.39	0.28	0.35
Al	1.99	2.01	1.99	1.99	2.00	2.02
Si	2.91	3.02	2.98	3.01	2.98	2.98
Ca	0.10	0.10	0.10	0.11	0.07	0.10
Mn	0.47	0.42	0.44	0.51	0.58	0.51
Fe	2.30	2.02	2.05	1.99	2.12	2.01
Mg/Fe	0.14	0.20	0.23	0.20	0.13	0.18
End-member proportions						
Almandine	0.67	0.68	0.65	0.66	0.68	0.67
Spessartine	0.15	0.14	0.15	0.17	0.19	0.17
Pyrope	0.10	0.14	0.16	0.13	0.09	0.12
Grossular	0.00	0.03	0.02	0.03	0.01	0.03
Andradite	0.03		0.01		0.01	

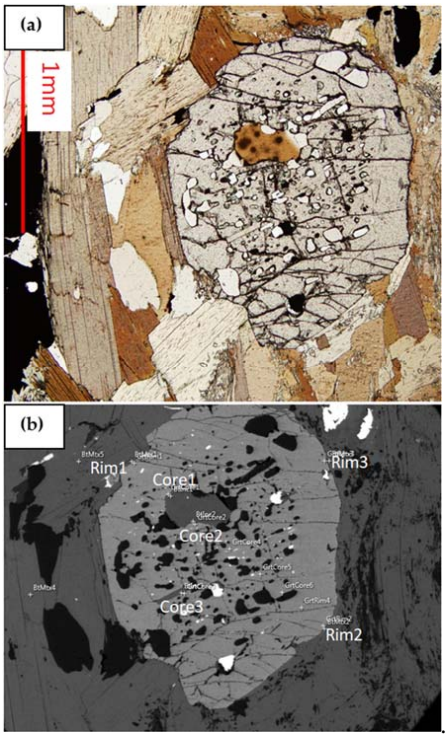

Figure 4. (**a**) Photomicrograph of garnet porphyroblast in biotite matrix from sample FD 01340. (**b**) Backscattered electron (BSE) image of garnet from sample FD 01340. Locations of EDS spot analyses across the diameter and at core and rim locations are shown (Table 1). Corresponding EDS chemical mapping images are provided in Figure S1 (Supplementary Materials).

3.2. Compositional Analysis Using Scanning Electron Microscopy

The compositions (Table 1) and textures of mineral assemblages (Figure 4b) were established using a Hitachi Su-70 Schottky Field Emission scanning electron microscope (SEM) at Lakehead University Instrumentation Laboratory (LUIL). It has a resolution of 1.0 nm at 15 kv which was the optimal output power used. Mineral compositions were obtained using the energy dispersive X-ray spectrometer (EDS) Oxford Aztec software package and the Mn-Hort (Si, Fe, Mn), Wollastonite (Ca), Jadeite (Al, Na), Apatite (P), and $SiTiO_3$ (Ti, Sr) standards.

3.3. In Situ Trace Element Analysis by LA-ICPMS

The laser ablation inductively coupled plasma mass spectrometer (LA-ICPMS) set-up at the University of Toronto consists of an NWR 193 UC laser ablation system coupled with an Agilent 7900 quadrupole ICPMS. The laser beam power was set to 10 Hz with a beam size of 40 µm. The GSD-1G and NIST 610 glass standards were used to bracket the sample analyses and monitor accuracy and reproducibility. Internal errors (1σ) on measurements were ~1% or better for major and minor elements, (e.g., Ca, Fe, Ti, Y), and 1 to 30% for trace elements (Table 2). Three millimeter-sized garnet crystals from the same polished thin section of FD 01340 were analyzed at 6 to 7 individual points spread in line every 150 µm across the crystals for selected major, minor, and trace elements by LA-ICPMS (Figures 5 and 6 and Table 2).

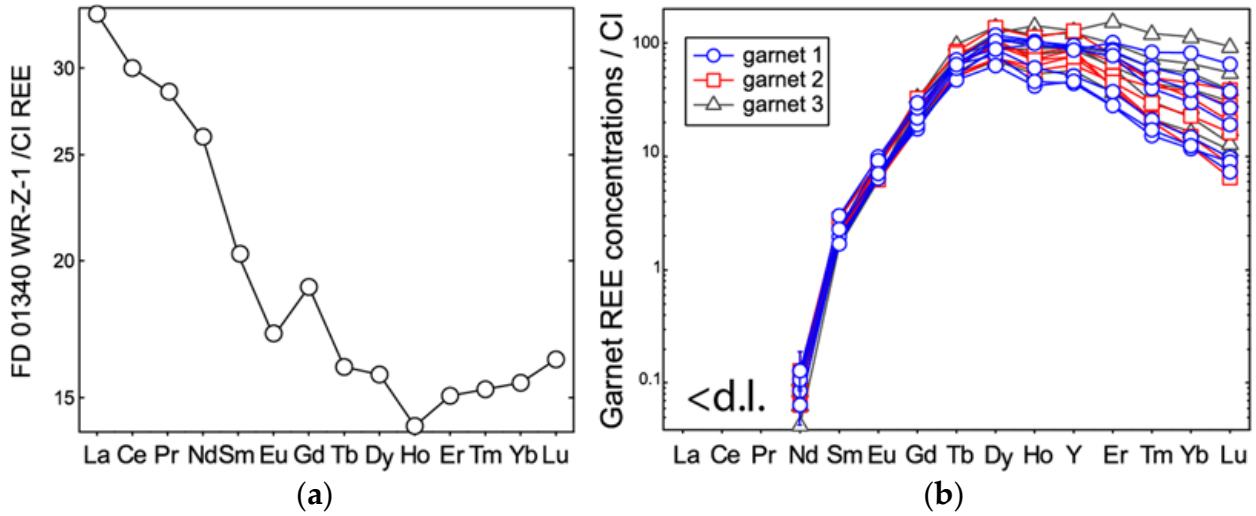

Figure 5. (**a**) REE concentrations of FD 01340 WR-Z-1 (5–10% 2SD) normalized to those of CI chondrites. (**b**) REE concentrations of garnet measured by LA-ICPMS normalized to those of CI chondrites. La, Ce, and Pr were under detection limits (<d.l.) of the LA-ICPMS system. Error measurements (2SD) were the largest for Nd (~30% 2SD), and smaller than symbol sizes for other REE (1–3% 2SD).

Table 2. LA-ICPMS elemental data for 3 selected garnets (6–7 spots per garnet crystal) normalized to 17.54% Si. Elements K, Rb, Sr, Ta, W, Pb, Th, and U were measured below detection limits. The session average %2SD errors for each element are indicated.

	%	%	%	%	µg/g	µg/g	µg/g	µg/g	µg/g	µg/g	µg/g	µg/g	µg/g	µg/g	µg/g	µg/g	µg/g	µg/g	µg/g	µg/g
Garnet Spot	**Mg**	**Al**	**Ca**	**Fe**	**Na**	**Ti**	**Y**	**Zr**	**Mo**	**Nd**	**Sm**	**Eu**	**Gd**	**Tb**	**Dy**	**Ho**	**Er**	**Tm**	**Yb**	**Lu**	**Hf**
1-1	2.2	10.9	0.63	22.5	60.4	13.6	124	1.3	0.48	0.05	0.32	0.39	3.3	1.8	20.4	5.0	15.3	2.0	13	1.5	0.04
1-2	2.6	10.6	0.61	21.7	77.2	15.0	72	3.3	0.38	0.05	0.42	0.53	5.5	2.4	20.3	3.1	5.6	0.49	2.3	0.22	0.06
1-3	2.6	10.4	0.61	21.3	67.1	15.7	62	4.5	0.38	0.05	0.32	0.49	4.9	2.2	17.8	2.3	4.1	0.36	1.8	0.19	0.10
1-4	2.6	10.4	0.62	21.1	61.3	16.6	125	3.9	0.46	0.03	0.25	0.37	4.3	2.4	26.6	5.3	11.2	0.93	4.5	0.42	0.08
1-5	2.6	10.3	0.61	20.9	62.2	13.8	132	1.6	0.38	0.04	0.23	0.34	4.0	2.1	24.7	5.2	12.5	1.4	7.5	0.82	0.03
1-6	2.5	10.3	0.61	21.0	58.6	14.3	120	2.7	0.41	0.05	0.27	0.33	3.7	2.0	23.5	5.0	11.4	1.2	5.7	0.59	0.06
1-7	2.3	10.3	0.62	21.4	85.8	12.4	64	4.5	0.49	0.04	0.23	0.35	3.5	1.6	14.3	2.1	4.2	0.40	1.9	0.16	0.09
2-1	2.1	9.8	0.66	20.3	60.8	12.5	103	2.1	0.38	0.04	0.27	0.31	3.2	1.6	16	3.1	7.4	0.93	5.5	0.59	0.05
2-2	2.4	9.8	0.60	20.2	69.2	15.7	173	5.8	0.39	0.04	0.31	0.44	5.5	2.7	30.1	5.5	11.3	1.0	4.8	0.43	0.08
2-3	2.4	9.8	0.66	20.2	54.1	13.2	124	2.8	0.28	0.04	0.24	0.36	4.1	2.1	20.8	4.0	9.9	1.1	6.5	0.83	0.05
2-4	2.5	10.0	0.67	20.6	63.6	17.2	119	6.2	0.31	0.05	0.38	0.45	5.9	2.7	23.9	3.6	5.9	0.47	1.8	0.14	0.11
2-5	2.4	10.1	0.66	20.7	64.6	16.1	104	3.8	0.38	0.03	0.28	0.43	4.7	2.2	21.4	3.5	6.3	0.50	2.2	0.18	0.07
2-6	2.1	10.2	0.70	21.1	68.1	11.9	88	2.9	0.35	0.03	0.28	0.36	3.8	1.8	16.3	2.9	6.6	0.68	3.4	0.35	0.06
3-1	2.1	10.1	0.64	20.9	66.3	13.7	78	3.7	0.53	0.02	0.25	0.32	3.4	1.7	15.5	2.6	5.4	0.49	2.4	0.24	0.08
3-2	2.5	10.0	0.65	20.4	58.8	15.9	125	2.8	0.30	0.05	0.28	0.31	3.5	1.8	19.4	4.4	11.9	1.4	8.0	0.84	0.05
3-3	2.5	10.1	0.65	20.3	66.1	16.7	176	2.1	0.41	0.05	0.31	0.35	4.6	2.5	27.2	7.1	22.5	2.8	17	2.0	0.04
3-4	2.5	10.1	0.66	20.4	47.3	14.9	168	1.4	0.40	0.02	0.22	0.32	5.7	3.2	31.0	5.8	14.5	1.7	9.7	1.2	0.03
3-5	2.5	10.1	0.70	20.5	65.0	21.0	119	1.7	0.44	0.04	0.4	0.45	6.1	2.6	21.9	3.9	9.1	1.0	5.8	0.66	0.04
3-6	2.5	10.0	0.67	20.1	57.6	17.1	130	3.5	0.38	0.04	0.29	0.41	5.3	2.4	24.7	4.5	8.7	0.70	3.2	0.28	0.07
3-7	2.6	10.5	0.68	21.1	85.0	14.9	119	2.6	0.39	0.03	0.3	0.36	4.0	2.0	21.7	4.2	8.8	0.85	4.1	0.38	0.06
% error (2SD)	1	0.9	1.7	1	5	4.5	1	3	12	29	12	5	3.1	1.8	1.4	1.5	1.7	2.6	2.5	2.6	30

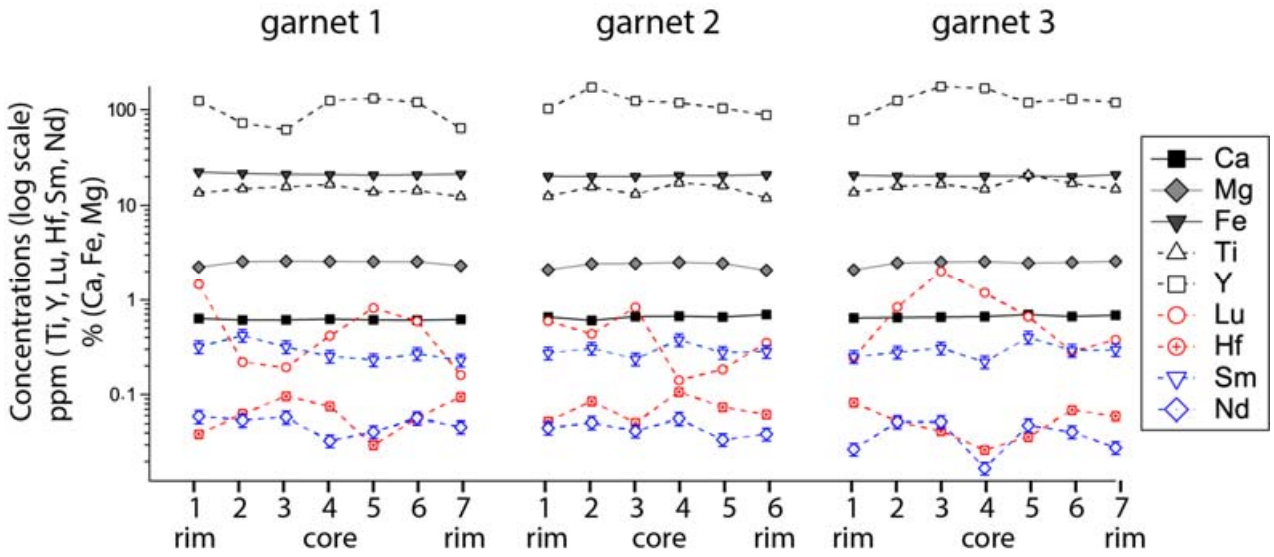

Figure 6. LA-ICPMS trace elemental composition of garnet transects from rim to core to rim of three individual crystals selected in the thin section (see further details in text and Table 2 for associated errors).

3.4. Whole-Rock Analysis of Fused Beads by ICP-OES

Several whole-rock powders of rock lithologies of the area, including three related garnet-biotite gneisses (but not FB 01340), were sent for commercial service analyses to Activation Laboratories Ltd. (Actlabs in Thunder Bay, Ontario). Fused glass beads were analyzed by inductively coupled plasma-optical emission spectrometry (ICP-OES) for major and minor element abundances.

3.5. ^{176}Lu-^{176}Hf Geochronology and REE Composition of FD01340 Garnet and Whole-Rock Fractions

Approximately 25 kg of rock from the channel sample was ground in a jaw crusher at the University of Western Ontario. A fine, homogenized whole-rock powder was produced in a stainless-steel mill. The remaining materials were crushed and sieved into three-grain fractions. Garnet grains were concentrated from the 125–250 µm fraction using a Frantz magnetic separator followed by heavy liquid density separation (methylene iodide, density approximately 3.2 g/cm^3) prior to further purification by handpicking in the GEOMETRIC Lab at the University of Western Ontario.

Three splits of whole-rock (WR) powder of sample FD 01340 between 0.15 to 0.65 g were dissolved following two methods. First, WR-Z-1 was dissolved in a concentrated HF-HNO_3 acid mixture using a Parr bomb vessel at 155 °C for 7 days (methods described in [17,18]) to ensure that all refractory minerals, including zircons, were fully dissolved. Second, for WR-WZ-2 and WR-WZ-3, a hot plate dissolution method at 120 °C and atmospheric pressure were utilized to avoid dissolving refractory minerals, which may not be in isotopic equilibrium and would also provide additional data points for the Lu-Hf internal isochron with a range of Lu/Hf ratios.

The whole-rock elemental rare earth element analysis and selected elemental ratios of WR-Z-1 were obtained using a quadrupole ICPMS Agilent 7700 from the Western Biotron analytical services (Table 3). The Lu and Hf concentrations obtained using the isotopic dilution method are reported in Table 4.

Table 3. Solution analysis by quadrupole ICPMS of whole-rock FD 01340 WR-Z-1 for rare earth element concentrations and selected elemental ratios.

Elements	**La**	**Ce**	**Pr**	**Nd**	**Sm**	**Eu**	**Gd**	**Tb**	**Dy**	**Ho**	**Er**	**Tm**	**Yb**	**Lu**
ppm	7.9	18	2.6	12	3.1	1.0	3.9	0.6	4.0	0.8	2.5	0.4	2.6	0.4
Selected ratios	**Hf/Zr**	**Nb/Ta**	**Lu/Hf**	**Th/U**	**Rb/Sr**									
	29	13	0.20	3.9	1.6									

Table 4. Lu-Hf isotope dilution data of garnet separates and whole rocks of sample FD 01340.

Dissolution Method	**FD 01340 Sub-Samples**	**Weight (g)**	**Lu (ppm)**	**Hf (ppm)**	**^{176}Lu/^{177}Hf**	**±2SE**	**^{176}Hf/^{177}Hf**	**±2SE**
Parr	whole-rock WR-Z-1	0.191	0.391	1.895	0.0293	0.0001	0.282690	0.000010
TT	whole-rock WR-WZ-2	0.151	0.351	0.747	0.0666	0.0001	0.284556	0.000008
TT	whole-rock WR-WZ-3	0.648	0.313	0.459	0.0968	0.0002	0.286075	0.000005
TT	garnet 1	0.102	2.048	0.733	0.3979	0.0008	0.301241	0.000007
TT	garnet 2	0.150	2.150	0.774	0.3952	0.0008	0.301089	0.000006

^{176}Hf/^{177}Hf ratios were normalized to ^{179}Hf/^{177}Hf = 0.7325 and to the recommended value of 0.282160 for the JMC 475 Hf standard to correct for instrumental mass bias and faraday cup efficiency. TT = table-top hot plate dissolution, Parr = acid digestion pressure vessels, Z = zircon, and WZ = without zircon. See text for further details.

Garnet fractions were prepared according to the methods described in Cheng et al. [19]. About 0.10 to 0.15 g of sieved grains were first acid washed in 1 M hydrochloric acid (HCl) at room temperature, sonicated for 5 min, then rinsed in Millipore H_2O, sonicated for 5 min, and water was pipetted off. Concentrated 14 M nitric acid (HNO_3) and 29 M hydrofluoric acid (HF) (1:10 of HNO_3:HF), were added to the beakers for acid digestion on hot plate and 120 °C for 24 h. Samples were dried, before being covered with perchloric acid evaporated at 150–180 °C. For whole-rock and garnets samples, the samples were redissolved in 6 M HCl and H_2O_2, solutions were dried once more and dissolved again in 6 M HCl. Mixed ^{176}Lu-^{180}Hf spike was finally added to the sample solutions, fluxed together, and once again dried to ensure sample-spike equilibration.

A detailed protocol for Hf-REE separation and purification is described in Bouvier et al. [17]. In summary, 8.5 mL cation Biorad AG50W-X8 200–400 mesh resin in PFA Teflon columns were used to separate HFSE from the matrix and REE fractions. Hafnium was further purified using an Eichrom Ln-spec resin chemistry protocol in teflon columns modified from Münker et al. [20] and Lu + Yb was subsequently separated from the rest of the REE on Ln-spec resin in quartz columns [17].

Teflon beakers used were PFA Savillex® and PTFE vessels for the Parr® bombs. Chemicals (HF, HNO_3, HCl, $HClO_4$, and H_2O_2) used during this protocol were Aristar Ultra from BDH or Plasma Pure Plus Optima Grade from SCP Science. Water was purified to a resistivity of 18.2 MΩ using a Millipore Advantage system and QPOD Element dispenser. Total analytical blanks were 20 pg for Hf and 5 pg for Lu, which are negligible.

Purified fractions of Hf and Lu (with ~20% Yb) were analyzed by plasma source mass spectrometry using an Aridus II nebulizer coupled with a Neptune Plus MC-ICP-MS at Laboratoire Magmas et Volcans, University of Clermont-Ferrand (France). The average ^{176}Hf/^{177}Hf ratios and two standard deviations (2SD) for the JMC 475 Hf isotopic standards measured in static mode (75 ratios) during analytical sessions were, respectively, 0.282160 ± 0.000009 (2SD, 10 ppb Hf) and 0.282154 ± 0.000008 (2SD, 20 ppb Hf). The Lu fractions of the samples were collected with part of the Yb and thus analyzed together to correct for interference and instrumental mass bias using the method described in Vervoort et al. [21]. External reproducibilities on isotopic ratios used for age calculations are ±0.000010 for ^{176}Hf/^{177}Hf and ±0.5% for Lu/Hf based on repeated measurements of BCR-2 standards using the same isotopic dilution method. The isotopic compositions and

elemental concentrations obtained by the isotopic dilution method for the whole-rock splits and garnet fractions are presented in Table 4. The epsilon unit for Hf (reported in Figure 7) is the deviation in parts per 10,000 relative to Chondrite Uniform Reservoir calculated at 2629 Ma using the CHUR Lu-Hf parameters from [17].

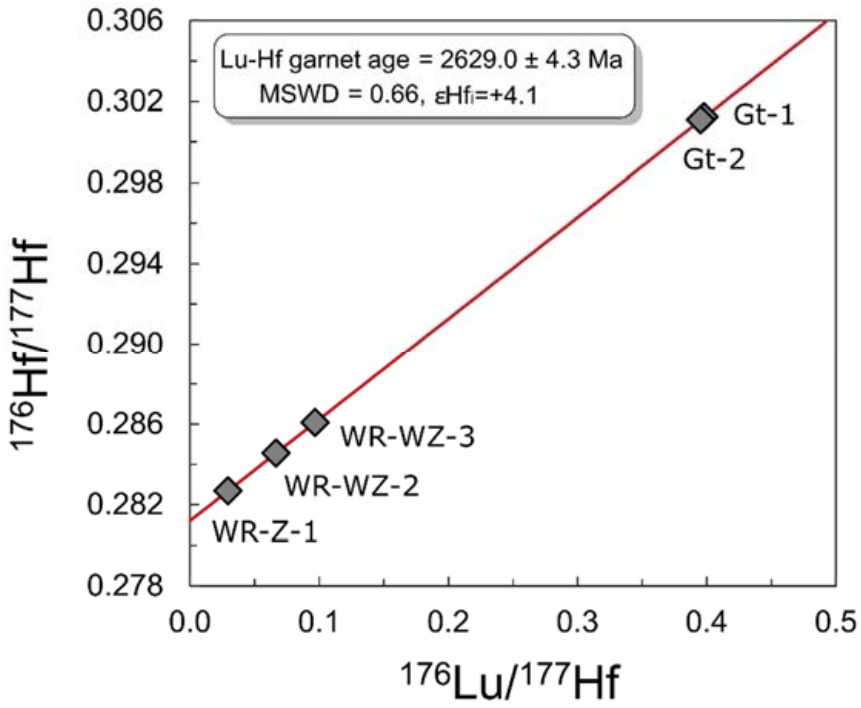

Figure 7. ^{176}Lu-^{176}Hf internal isochron of sample FD 01340 with two garnet separates (Gt-1 and -2) and three whole-rock samples (WR-Z-1 dissolved with zircons, WR-WZ-1 and -2 without zircons). Isochron regression line and error envelope (in red) represent a 95% confidence level and appear as a line. Symbols are oversized compared to external errors on isotopic ratios (Table 2).

4. Results

4.1. Garnet Composition

Inclusions of quartz and biotite are abundant in garnet (Figure 5a). Garnet grains appear unzoned for major elements (Figure 5b). Spot analysis using a Scanning Electron Microscope (SEM) at intervals across each garnet grain shows that Fe/Mg ratios (0.14–0.23; Table 1) are consistent from the core to the rim [8]. Garnet grains are dominantly almandine (60 to 70%), with moderate components of pyrope (15%), spessartine (15%), and minor components of andradite (<5%) and grossular (<3%). The specific mineral formula for Borden garnet was determined to be $Fe_2Mg_{0.5}Mn_{0.4}Ca_{0.1}Al_2$ $(SiO_4)_3$.

Using LA-ICPMS analysis, we obtained elemental transects across three individual garnet crystals of the thin section of FD 01340. The major element (Mg, Fe, Ca) concentrations measured by LA-ICPMS of the garnet crystals from core to rim are similar to those measured by SEM-EDS analysis. Elements such as Rb, Sr, Ba, La, Ce, Pr, Ta, W, Au, Pb, Th, and U were measured below detection limits of the LA-ICPMS system (~0.01 ppm) in garnet and are thus not reported. All three garnet crystals have similar and overlapping trace element concentrations. Trace elements such as Mo or Ti are also mostly homogeneous throughout the crystals (Table 2), while more variations are found for HREE, Y, Zr, and Hf (Table 2). The Zr/Hf varies from 32 to 69 with an average of 50 ± 15 (2SD), slightly super-chondritic (~35–40), indicating minor contribution from zircon inclusions besides potentially in spot #2-2. The average elemental ratios vary as such: Lu/Hf = 14 ± 29, Sm/Nd = 8 ± 5, and Lu/Nd = 17 ± 35 (2SD) indicated larger variability for HREE abundances which could be attributed to minute amounts of accessory phases such as monazite or xenotime, possibly so small that were not observed by SEM. There is slight enrichment in Y, and similarly in

Lu at two orders of magnitude lower concentrations, in the center regions of the garnets. When normalized to CI chondrite elemental abundances, the garnets are all depleted in LREE compared to HREE without any Eu anomaly, with Dy contents of 60–140 chondrite units, and $(Dy/Yb)_N$ = ~1–5 and $(Nd/Yb)_N$ = ~0.01–0.0005. The strongest enrichment is found for Tb, Dy, Ho, and Y and decreases towards Lu in some locations. These spots are not systematically associated with their location respective to the core or rim within the three garnet crystals analyzed (Figure 6) which supports the idea that inclusions were randomly picked up during laser ablation spot analysis.

4.2. Whole-Rock Elemental Analysis

The REE concentrations of the whole-rock WR-Z-1 and individual garnet LA-ICPMS analyses, when normalized to concentrations measured in CI chondrites [22], are presented in Figure 5a,b and provided in Tables 2 and 3. The composition of the whole-rock sample WR-Z-1 (Table 3) indicates a low enrichment in REE (15–35 × CI chondrites) with (La/Yb)N = 2 and a small $(Eu/Eu^*)_N$ = 0.9. Elemental ratios are slightly sub-chondritic for Zr/Hf = 29, Nb/Ta = 13, slightly super-chondritic for Th/U = 3.9, to super-chondritic for Rb/Sr = 1.6.

The whole-rock compositions of three different garnet biotite gneisses (but not FD 01340) analyzed from drill cores have 55.6 to 58.5% SiO_2, 13.8 to 15.5% Al_2O_3, 11.0–13.8% Fe_2O_3, 3.3–4.3% MgO, 1.1–2.3% CaO, 0.7–1.0 TiO_2, 2.3–2.5% Na_2O and 3.4–3.5% K_2O indicating an Al-rich, alkaline and basaltic nature for the protolith of these rocks.

4.3. Lu-Hf Radiometric Dating of Garnet

The Lu-Hf isotopic compositions of whole-rock splits and garnet separate from sample FD 01340 and their Lu-Hf internal isochron age are presented in Table 4 and Figure 7. Garnets used for Lu-Hf radiometric dating were from the same hand samples used for thin section and LA-ICPMS analyses documented in Figures 4, 5b and 6, respectively. The Lu-Hf isotopic data were obtained from two 100 mg garnet splits and three whole-rock splits (with and without dissolving zircons) of sample FD 01340 (Table 4). These fractions yield a precise internal isochron age at 2629.0 ± 4.3 Ma (with an initial $^{176}Hf/^{177}Hf$ = 0.281210 ± 0.000010 and MSWD = 0.66) from five data points. This age is identical within error to the Lu-Hf isochron age of 2630.4 ± 4.7 Ma (with an initial $^{176}Hf/^{177}Hf$ = 0.281204 ± 0.000013 and MSWD = 0.16) when the whole rock dissolved with zircons (WR-Z-1) is not included in the age calculation (Figure 7). The initial Hf isotopic composition of the sillimanite-garnet-biotite gneiss corresponds to εHfi = +4.1 which, indicates that the protolith of this rock was derived from a long-term depleted (high Lu/Hf) reservoir compared to the primitive mantle (CHUR [17], which by definition has a value of 0).

5. Discussion

5.1. Metamorphism

The description of the metamorphism is critical to interpreting the significance of the Lu-Hf age of the garnet formation in regards to the timing of the gold mineralization event. The sillimanite-garnet-biotite gneiss represents an upper-amphibolite-facies dominated by a mineral assemblage composed of quartz, plagioclase, biotite, almandine garnet, and fibrolite. The stable mineral assemblage of coarse sillimanite with K-feldspar, quartz, and a complete lack of muscovite represents the peak conditions of granulite-facies metamorphism. The presence of fibrolite and coarse sillimanite suggests secondary growth of sillimanite during amphibolite-facies temperatures during retrograde metamorphism.

Similarly, the amphibolite (±garnet) contains the stable mineral assemblage of hornblende, plagioclase, and garnet representing the amphibolite-facies of metamorphism. Relict microlithons of clinopyroxene and orthopyroxene representing the granulite facies of metamorphism are also present within mineralized amphibolite. The dominant stable amphibolite-facies mineral assemblage, in addition to relict granulite-facies

lithons, suggests polymetamorphism to the amphibolite facies after peak granulite-facies metamorphic conditions.

The mineralized mafic amphibolite (±garnet) and sillimanite-garnet-biotite gneiss units display evidence of stable retrograde amphibolite facies mineral assemblages and relict lithons of granulite-facies assemblages [8]. Granulite-facies assemblages are less reactive and more competent during deformation at amphibolite-facies temperatures resulting in abundant microfractures in response to differential stress. While in contrast, the ductilely deforming amphibolite assemblages of hornblende and garnet-biotite gneiss with biotite accommodate rehydration reactions and increased response to ductile deformation. The granulite-facies rocks are more akin to low-strain domains in anastomosing shear zones. Retrograde metamorphic reactions during deformation caused reaction softening so that the granulite-facies lithons were more competent than the rock undergoing retrograde metamorphism.

In the case of the Borden Gold deposit, lenses of relict granulite-facies rocks were more competent than the surrounding retrograde amphibolite-facies lithologies at the time of retrograde metamorphism, producing the requisite conditions for localized brittle deformation and mineralization during dominantly ductile shear-zone deformation.

5.2. Lithology

The sillimanite-garnet-biotite gneiss can be interpreted as a metasedimentary unit due to the abundance of aluminous minerals. The nature of these sediments can be further discussed in light of their geochemistry. The Lu-Hf internal isochron of the sillimanite-garnet-biotite gneiss on the Discovery Outcrop provides an initial $^{176}Hf/^{177}Hf$ of 0.281204 ± 0.000013. This initial Hf isotopic composition corresponds to an εHf_i of +4.1 (Figure 7). This value falls between the chondritic and depleted mantle compositions and is similar to the range of values (+2 to +5) found in Archean zircons of magmatic intrusions (2670–2750 Ma) from the Abitibi and Wawa sub-provinces [5,23]. Such Hf isotopic composition suggests that the source of this metasediment had a mafic provenance which would be more commonly formed in the Archean. The elemental ratios such as Zr/Hf, Nb/Zr and Th/U (Table 3) of FD 01340 are in identical proportions with the chondritic values (Zr/Hf = 34.2 ± 0.3 and Nb/Ta = 17.6 ± 1.0; [24]). Zr/Hf can vary in magmatic systems due to the melting process in the deep mantle, (e.g., OIB source), or the crystallization of ferromagnesian minerals such as clinopyroxene, biotite, sphene, or amphibole [25], or finally mineral sorting such as zircons in detrital sediments. The near chondritic values found for FD 01340 support mafic juvenile rocks, not evolved, as the sedimentary source prior to metamorphism. Such a source could be genetically related to Archean intrusions derived from a long-term depleted (super-chondritic Lu/Hf) mantle. Such a source could be similar in elemental and mantle source isotopic composition to other metasediments reported in the Abitibi, and contrast in composition with metasediments from the Pontiac province suggesting different provenances [6]. Alternatively, the magma source of the protolith could have been potentially derived from a crustal source reservoir previously depleted in incompatible elements such as in the lower crust. Such scenarios have been previously put forward to explain the composition of the granitic intrusions in the area by remelting mafic sources [5].

5.3. Geochronology

Uranium-Pb dating of zircon and monazite from high-grade metamorphic rocks in the Kapuskasing Structural Zone has identified that the regional granulite-facies metamorphism took place at mid-crustal levels of the southern Superior craton ca. 2660 Ma [16]. The earliest time of garnet formation was therefore taken as ~2.66 Ga based on the age of the oldest metamorphic zircon in retrograde mafic granulite (Moser, 1994). Zircon in the KSZ yields dates of metamorphism in the range ca. 2690 to 2580 Ma, with the most commonly observed metamorphic zircon formation occurring at 2660 Ma in granulite-facies mafic gneiss (Figure 8).

Pervical and West [26] noted that combined U-Pb and K-Ar geochronology suggest the possibility of an event involving some uplift in parts of the KSZ at ~2630 Ma. Mylonitic monazites near the eastern margin of the KSZ have 2628 ± 2 Ma ages. Pegmatites cutting high-strain gneisses of the KSZ have an identical U-Pb zircon age at ~2629 Ma (Figure 8). Granitic sheets near the Borden Lake Belt were emplaced around 2633 Ma. An orthopyroxene-bearing leucosome in paragneiss from the southeastern Chapleau block formed in 2627 Ma. In the northern Chapleau block, a K-Ar hornblende age of 2630 Ma suggests cooling to below the hornblende closing temperature (~550 °C) by this time. The oldest metamorphic zircon age of 2696 Ma comes from the northern Chapleau block. The K-Ar age suggests that the cycle of granulite-facies metamorphism and cooling occurred earlier in rocks of the northern Chapleau block than elsewhere. Metamorphic zircon dates in the 2630 Ma range from further south indicate active high-grade metamorphism at the same time that granulites in the north were cooling (Figure 8). There is therefore a major thermotectonic event recorded at 2.63 Ga within the KSZ. It is significant that the Lu-Hf chronology of garnet forming in the Borden paragneiss is coeval with this major event. The closure temperature of the Lu–Hf system is generally accepted to be >700 °C [27], which is intermediate to the Ti-in-zircon temperatures proposed for overgrown rims of the detrital zircons between 660 to 706 °C [2]. Garnet grains have higher concentrations of radioactive isotopes, (i.e., Lu or Y with a similar HREE behavior, Figure 6) in the core in the early growth stages, followed by a decrease during the later growth stages. This suggests that the Lu-Hf age is biased towards prograde growth of garnet. In contrast, if the radioactive isotope was concentrated in the rims of the garnet, the age would be biased towards the end of garnet growth [28]. The time sequence of events between initiation of the greenstone belt volcanism and subsequent metamorphism, in a tectonic setting involving crustal burial and thickening, and terminating in fluid-assisted retrograde deformation in the KSZ controlling the gold mineralization [8], is summarized in Figure 8.

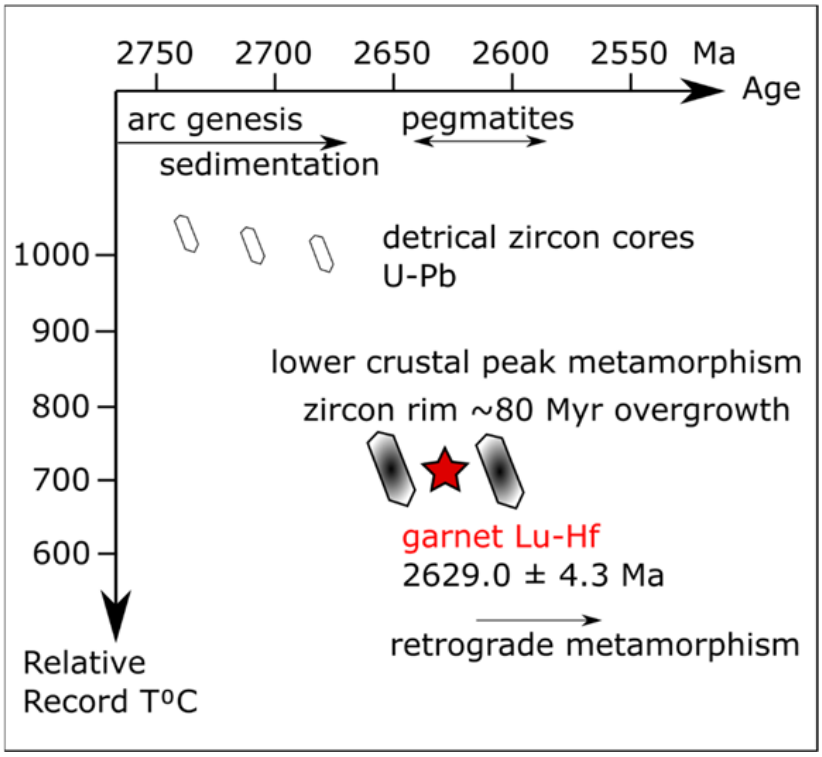

Figure 8. Summary of the igneous and metamorphic events of the Kapuskasing Structural Zone obtained from U-Pb detrital zircon ages and Ti-in-zircon temperatures for overgrowth rims (660–706 °C) [2,4], and Lu-Hf garnet age (this study) and corresponding closure temperature, which is generally accepted >700 °C [27], of Borden Lake metasediments.

Moser [14] hypothesized that protracted radial overgrowth of zircon appears to have been most frequent ca. 2620 Ma, when temperatures were above 650 °C, and the events coincided with boudinage in the lower crust and crustal-scale fluid flow along with brittle structural breaks at higher levels [4]. Our new constraints are based on the Lu-Hf garnet date of 2629 Ma, suggesting that the age of granulite-facies metamorphism is consistent with Krogh's [4] and Moser et al.'s [2] U-Pb dates of zircons for high-temperature metamorphism and rim overgrowths (Figure 8). This also supports the hypothesis that the exhumation of the KSZ began during this time.

The retrograde metamorphism of these lithologies is critical to the structural control of mineralization at this deposit. The association of gold with retrograde amphibolite-facies metamorphism suggests that mineralization at the Borden Gold deposit coincides with exhumation and cooling in the late Archean after ~2629 Ma. Because lenses of relict granulite-facies rock were more competent than surrounding retrograde amphibolite-facies lithologies, they produced the requisite conditions for localized brittle deformation. Shear fabrics in garnet-biotite gneiss appear to be formed during and after peak metamorphism, producing low-strain environments favorable for gold mineralization.

6. Conclusions

Unzoned garnet from the Discovery Outcrop has homogeneous Fe/Mg and minor element compositions from the core to the rim preserving peak to retrograde metamorphic diffusion. This indicates that garnet equilibration was reached during peak metamorphism and garnet growth took place during prograde metamorphism to the granulite facies. The abundance of aluminous minerals in the sillimanite-garnet biotite gneiss and the initial Hf radiogenic isotopic signature (εHf_i = +4.1) suggest that the protolith may have had a sedimentary source derived predominantly by erosion of juvenile magmatic rocks related to the Abitibi Archean intrusions.

Structure and microstructure are the controlling factors in gold mineralization within the Borden Gold deposit. Foliated biotite surrounding competent garnet is commonly deflected around the grain. Sillimanite typically occurs as fibrolite needles on the grain boundaries of biotite and quartz. Coarse prismatic sillimanite grains with K-feldspar occur in relict lithons within the gneiss indicating the second sillimanite isograd was reached during peak granulite-facies metamorphism. Visible gold is observed in microscopic low-strain shadows caused by mineral competency contrasts between rigid garnet and sillimanite compared to biotite and quartz. Relict granulite-facies lithons appear to have behaved competently during ductile deformation at lower temperatures. Research on the property to date provides evidence for gold mineralization in association with brittle-ductile heterogeneous strain and rheological competency contrasts between minerals on the microstructural scale as well as lithologies on the deposit scale. Gold mineralization appears to be contemporaneous with retrograde metamorphism of granulite-facies lithologies to amphibolite-facies, and with ductile deformation of the retrograde amphibolite-facies units after the crystallization of garnet at peak metamorphism, thus post-dating 2629.0 ± 4.3 Ma. These new Lu-Hf geochronological results on garnet are consistent with the youngest population of overgrown zircon U-Pb ages measured in the paragneiss [4].

Supplementary Materials: The following are available online at https://www.mdpi.com/article/10.3390/geosciences12050218/s1, Figure S1: Selected elemental EDS maps of garnet in sample FD 01340.

Author Contributions: Conceptualization, D.L., M.L.H. and A.B.; methodology, D.L. and A.B.; validation, D.L., M.L.H. and A.B.; formal analysis, D.L. and A.B.; investigation, D.L. and A.B.; data curation, D.L. and A.B.; writing—Original draft preparation, D.L. and A.B.; writing—Review and editing, D.L., M.L.H. and A.B.; supervision, M.L.H.; funding acquisition, M.L.H. and A.B. All authors have read and agreed to the published version of the manuscript.

Funding: This MSc thesis research was funded by David Palmer and Probe Mines Ltd. To D.L. and M.L.H., and supported by the Canada Foundation for Innovation JELF (grant number 33353), and NSERC Canada Research Chairs (950-229061) programs to A.B.

Institutional Review Board Statement: Not applicable.

Informed Consent Statement: Not applicable.

Data Availability Statement: The data presented in this study are available in the article.

Acknowledgments: We thank A. Van Kessel at Western, M. Gannoun at UCA, and Z. Zajacz at UT for their assistance during analytical sessions. We acknowledge the proficient editorial handling by Assistant Editors, as well as three anonymous reviewers for in-depth reviews and suggestions, which greatly improved the clarity and implications of our work.

Conflicts of Interest: The authors declare no conflict of interest. The funders had no role in the design of the study; in the collection, analyses, or interpretation of data; in the writing of the manuscript, or in the decision to publish the results.

References

1. Corfu, F.; Davis, D. AU–Pb geochronological framework for the western Superior Province. In *The Geology of Ontario*; Thurston, P.C., Williams, H.R., Sutcliffe, R.H., Stott, G.M., Eds.; Special Volume 4, Part 2; Ontario Geological Survey: Toronto, ON, Canada, 1992; pp. 1335–1346.
2. Moser, D.E.; Bowman, J.R.; Wooden, J.; Valley, J.W.; Mazdab, F.; Kita, N. Creation of a continent recorded in zircon zoning. *Geology* **2008**, *36*, 239–242. [CrossRef]
3. Percival, J.; Krogh, T. U–Pb zircon geochronology of the Kapuskasing structural zone and vicinity in the Chapleau–Foleyet area, Ontario. *Can. J. Earth Sci.* **1983**, *20*, 830–843. [CrossRef]
4. Krogh, T.E. High precision U-Pb ages for granulite metamorphism and deformation in the Archean Kapuskasing structural zone, Ontario: Implications for structure and development of the lower crust. *Earth Planet. Sci. Lett.* **1993**, *119*, 1–18. [CrossRef]
5. Ketchum, J.W.F.; Ayer, J.A.; Van Breemen, O.; Pearson, N.J. Pericontinental Crustal Growth of the Southwestern Abitibi Subprovince, Canada—U-Pb, Hf, and Nd Isotope Evidence. *Econ. Geol. Bull. Soc. Econ. Geol.* **2008**, *103*, 1151–1184. [CrossRef]
6. Feng, R.; Kerrich, R.; Maas, R. Geochemical, oxygen, and neodymium isotope compositions of metasediments from the Abitibi greenstone belt and Pontiac Subprovince, Canada: Evidence for ancient crust and Archean terrane juxtaposition *Geochim. Cosmochim. Acta* **1993**, *57*, 641–658. [CrossRef]
7. Vervoort, J.D.; Patchett, P.J.; Blichert-Toft, J.; Albarède, F. Relationships between Lu-Hf and Sm-Nd isotopic systems in the global sedimentary system. Earth Planet. *Sci. Lett.* **1999**, *168*, 79–99.
8. LaFontaine, D. Structural and Metamorphic Control on the Borden Gold Deposit, Chapleau, Ontario. Master's Thesis, Lakehead University, Thunder Bay, ON, Canada, 2016.
9. Watson, J.V. A Discussion on the evolution of the Precambrian crust-Effects of reworking on high-grade gneiss complexes. *Philos. Trans. R. Soc. Lond. Ser. A Math. Phys. Sci.* **1973**, *273*, 443–455.
10. Sutton, J.; Watson, J.V. Tectonic evolution of continents in early Proterozoic times. *Nature* **1974**, *247*, 433–435. [CrossRef]
11. Piper, J. A Discussion on global tectonics in Proterozoic times-Palaeomagnetic evidence for a Proterozoic super-continent. *Philos. Trans. R. Soc. Lond. Ser. A Math. Phys. Sci.* **1976**, *280*, 469–490.
12. Bursnall, J.; Leclair, A.; Moser, D.; Percival, J. Structural correlation within the Kapuskasing uplift. *Can. J. Earth Sci.* **1994**, *31*, 1081–1095. [CrossRef]
13. Heather, K.; Percival, J.; Moser, D.; Bleeker, W. Tectonics and metallogeny of Archean crust in the Abitibi-Kapuskasing-Wawa region. In *Geological Survey of Canada, Open File 3141*; Natural Resources Canada: Ottawa, ON, Canada, 1995.
14. Moser, D. The geology and structure of the mid-crustal Wawa gneiss domain: A key to understanding tectonic variation with depth and time in the late Archean Abitibi–Wawa orogen. *Can. J. Earth Sci.* **1994**, *31*, 1064–1080. [CrossRef]
15. Percival, J.A. *Field Trip 16 Guidebook: The Kapuskasing Uplift: Archean Greenstones and Granulites*; Geological Association of Canada: St. John's, NL, Canada, 1986.
16. Krogh, T.; Moser, D. U-Pb zircon and monazite ages from the Kapuskasing uplift: Age constraints on deformation within the Ivanhoe Lake fault zone. *Can. J. Earth Sci.* **1994**, *31*, 1096–1103. [CrossRef]
17. Bouvier, A.; Vervoort, J.D.; Patchett, P.J. The Lu-Hf and Sm-Nd isotopic composition of CHUR: Constraints from unequilibrated chondrites and implications for the bulk composition of terrestrial planets. *Earth Planet. Sci. Lett.* **2008**, *273*, 48–57. [CrossRef]
18. Bouvier, A.; Boyet, M. Primitive Solar System materials and Earth share a common initial ^{142}Nd abundance. *Nature* **2016**, *537*, 399–402. [CrossRef]
19. Cheng, H.; King, R.; Nakamura, E.; Vervoort, J.; Zhou, Z. Coupled Lu–Hf and Sm–Nd geochronology constrains garnet growth in ultra-high-pressure eclogites from the Dabie orogen. *J. Metamorph. Geol.* **2008**, *26*, 741–758. [CrossRef]
20. Münker, C.; Weyer, S.; Scherer, E.E.; Mezger, K. Separation of high field strength elements (Nb, Ta, Zr, Hf) and Lu from rock samples for MC-ICPMS measurements. *Geochem. Geophys. Geosyst.* **2001**, *2*. [CrossRef]
21. Vervoort, J.D.; Patchett, P.J.; Söderlund, U.; Baker, M. Isotopic composition of Yb and the determination of Lu concentrations and Lu/Hf ratios by isotope dilution using MC-ICPMS. *Geochim. Geophys. Geosys.* **2004**, *5*. [CrossRef]
22. Barrat, J.A.; Zanda, B.; Moynier, F.; Bollinger, C.; Liorzou, C.; Bayon, G. Geochemistry of CI chondrites: Major and trace elements, and Cu and Zn Isotopes. *Geochim. Cosmochim. Acta* **2012**, *83*, 79–92. [CrossRef]

23. Corfu, F.; Noble, S.R. Genesis of the southern Abitibi greenstone belt, Superior Province, Canada: Evidence from zircon Hf isotope analyses using a single filament technique. *Geochim. Cosmochim. Acta* **1992**, *56*, 2081–2097. [CrossRef]
24. Weyer, S.; Münker, C.; Rehkämper, M.; Mezger, K. Determination of ultra-low Nb, Ta, Zr and Hf concentrations and the chondritic Zr/Hf and Nb/Ta ratios by isotope dilution analyses with multiple collector ICP-MS. *Chem. Geol.* **2002**, *187*, 295–313. [CrossRef]
25. David, K.; Schiano, P.; Allegre, C. Assessment of the Zr/Hf fractionation in oceanic basalts and continental materials during petrogenetic processes. *Earth Planet. Sci. Lett.* **2000**, *178*, 285–301. [CrossRef]
26. Percival, J.A.; West, G.F. The Kapuskasing uplift: A geological and geophysical synthesis. *Can. J. Earth Sci.* **1994**, *31*, 1256–1286. [CrossRef]
27. Smit, M.A.; Scherer, E.E.; Mezger, K. Lu–Hf and Sm–Nd garnet geochronology: Chronometric closure and implications for dating petrological processes. *Earth Planet. Sci. Lett.* **2013**, *381*, 222–233. [CrossRef]
28. Parmenter, S.; Ivanic, T.J.; Korhonen, F.J.; Bouvier, A.; Kendrick, J.L.; Yakymchuk, C. Metamorphism of the Mougooderra Formation: Implications for Neoarchean tectonics in the western Youanmi Terrane, Yilgarn Craton. *Precambrian Res.* **2020**, *350*, 105862. [CrossRef]